Publications

8-25-2016

New Halo White Dwarf Candidates in the Sloan Digital Sky Survey

Kyra Dame
University of Oklahoma, kyra.c.dame-1@ou.edu

A. Gianninas
University of Oklahoma

Mukremin Kilic
University of Oklahoma

Jeffrey A. Munn
US Naval Observatory

Warren R. Brown
Smithsonian Astrophysical Observatory

See next page for additional authors

Scholarly Commons Citation

Authors

Kyra Dame, A. Gianninas, Mukremin Kilic, Jeffrey A. Munn, Warren R. Brown, Kurtis A. Williams, Ted von Hippel, and Hugh C. Harris

New halo white dwarf candidates in the Sloan Digital Sky Survey

Kyra Dame,[1]★ A. Gianninas,[1]★ Mukremin Kilic,[1]★ Jeffrey A. Munn,[2]
Warren R. Brown,[3] Kurtis A. Williams,[4] Ted von Hippel[5] and Hugh C. Harris[2]

[1]*Homer L. Dodge Department of Physics and Astronomy, University of Oklahoma, 440 W. Brooks St, Norman, OK 73019, USA*
[2]*US Naval Observatory, Flagstaff Station, 10391 W. Naval Observatory Road, Flagstaff, AZ 86005, USA*
[3]*Smithsonian Astrophysical Observatory, 60 Garden St., Cambridge, MA 02138, USA*
[4]*Department of Physics and Astronomy, Texas A&M University-Commerce, PO Box 3011, Commerce, TX 75429, USA*
[5]*Embry-Riddle Aeronautical University, Physical Sciences, 600 South Clyde Morris Boulevard, Daytona Beach, FL 32114-3900, USA*

ABSTRACT

We present optical spectroscopy and near-infrared photometry of 57 faint ($g = 19$–22) high proper motion white dwarfs identified through repeat imaging of $\approx$3100 deg^2 of the Sloan Digital Sky Survey footprint by Munn et al. We use *ugriz* and *JH* photometry to perform a model atmosphere analysis, and identify 10 ultracool white dwarfs with $T_{\rm eff} < 4000$ K, including the coolest pure H atmosphere white dwarf currently known, J1657+2638, with $T_{\rm eff} = 3550 \pm 100$ K. The majority of the objects with cooling ages larger than 9 Gyr display thick disc kinematics and constrain the age of the thick disc to $\geq$11 Gyr. There are four white dwarfs in our sample with large tangential velocities ($v_{\rm tan} > 120$ km s^{-1}) and *UVW* velocities that are more consistent with the halo than the Galactic disc. For typical 0.6 M$_\odot$ white dwarfs, the cooling ages for these halo candidates range from 2.3 to 8.5 Gyr. However, the total main-sequence+white dwarf cooling ages of these stars would be consistent with the Galactic halo if they are slightly undermassive. Given the magnitude limits of the current large-scale surveys, many of the coolest and oldest white dwarfs remain undiscovered in the solar neighbourhood, but upcoming surveys such as *Gaia* and the Large Synoptic Survey Telescope should find many of these elusive thick disc and halo white dwarfs.

Key words: techniques: photometric – stars: atmospheres – stars: evolution – white dwarfs.

1 INTRODUCTION

As the remnants of some of the oldest stars in the galaxy, cool white dwarfs offer an independent method for dating different Galactic populations and constraining their star formation history (Winget et al. 1987; Liebert, Dahn & Monet 1988). The current best estimates for the ages of the Galactic thin and thick discs are 8 ± 1.5 Gyr (Leggett, Ruiz & Bergeron 1998; Harris et al. 2006) and $\geq$10 Gyr (Gianninas et al. 2015), respectively. Extended *Hubble Space Telescope* observing campaigns on 47 Tuc, M4, and NGC 6397 revealed the end of the white dwarf cooling sequence in these globular clusters (Hansen et al. 2004, 2007; Kalirai et al. 2012), which reveal an age spread of 11–13 Gyr for the Galactic halo (Campos et al. 2016).

Field white dwarfs provide additional and superior information on the age and age spread of the Galactic disc and halo. Recent large-scale surveys such as the Sloan Digital Sky Survey (SDSS)

have found many cool field white dwarfs (Gates et al. 2004; Harris et al. 2006, 2008; Kilic et al. 2006, 2010b; Vidrih et al. 2007; Tremblay et al. 2014; Gianninas et al. 2015). These stars are far closer and brighter than those found in globular clusters, allowing for relatively easy optical and infrared observations in multiple bands from ground-based telescopes. Modelling the spectral energy distributions (SEDs) of these white dwarfs provides excellent constraints on their atmospheric composition and cooling ages and gives us an alternate method for calibrating the white dwarf cooling sequences of globular clusters. However, there are only a handful of nearby halo white dwarfs currently known.

Kalirai (2012) use four field white dwarfs with halo kinematics to derive an age of 11.4 ± 0.7 Gyr for the inner halo. These four stars are warm enough to show Balmer absorption lines, which enable precise constraints on their surface gravity, mass, temperature, and cooling ages. The ESO SN Ia Progenitor Survey (SPY) project found 12 halo members with ages consistent with a halo age $\approx$11 Gyr in a sample of 634 DA white dwarfs. These have accurate radial velocities determined from Balmer absorption lines, allowing for the determination of accurate 3D space velocities (Pauli

★E-mail: kyra.c.dame-1@ou.edu (KD); alex.gianninas@gmail.com (AG); mukreminkilic@gmail.com (MK)

et al. 2003, 2006; Richter, Heber & Napiwotzki 2007). Similarly, Kilic et al. (2012) use optical and infrared photometry and parallax observations of two cool white dwarfs with halo kinematics, WD 0346+246 and SDSS J110217.48+411315.4 to derive an age of 11.0–11.5 Gyr for the local halo.

Ongoing and future photometric and astrometric surveys like the Panoramic Survey Telescope and Rapid Response System (Tonry et al. 2012), Palomar Transient Factory (Rau et al. 2009), the Large Synoptic Survey Telescope (LSST), and the *Gaia* mission will significantly increase the number of field white dwarfs known. Previously, Liebert et al. (2007) performed a targeted proper motion survey for identifying thick disc and halo white dwarfs in the solar neighbourhood. Munn et al. (2014) present the proper motion catalogue from this survey, which includes ≈ 3100 deg^2 of sky observed at the Steward Observatory Bok 90-inch telescope and the U.S. Naval Observatory Flagstaff Station 1.3-m telescope. Kilic et al. (2010a) presented three halo white dwarf candidates identified in this survey, with ages of 10–11 Gyr. Here we present follow-up observations and model atmosphere analysis of 54 additional high proper motion white dwarfs identified in this survey. We find seven new ultracool ($T_{\mathrm{eff}} < 4000$ K) white dwarfs and three new halo white dwarf candidates. We discuss the details of our observations in Section 2, and the model atmosphere fits in Section 3. We present the kinematic analysis of our sample in Section 4, and conclude in Section 5.

2 TARGET SELECTION AND OBSERVATIONS

2.1 The reduced proper motion diagram

Reduced proper motion is defined as $H = m + 5\log \mu + 5$ (where μ is the proper motion and m is the apparent magnitude), which is equivalent to $M + 5\log V_{\mathrm{tan}} - 3.379$. Hence, reduced proper motion can be used to identify samples with similar kinematics, like the disc or halo white dwarf population. Kilic et al. (2006, 2010b) demonstrate that the reduced proper motion diagram provides a clean sample of white dwarfs, with contamination rates of 1 per cent from halo subdwarfs. Fig. 1 displays the reduced proper motion diagram for a portion of the sky covered by the Munn et al. (2014) proper motion survey. Going from left to right, three distinct populations of objects are clearly visible in this diagram; white dwarfs, halo subdwarfs, and disc dwarfs. The solid lines show the predicted evolutionary sequences for $\log g = 8$ white dwarfs with $V_{\mathrm{tan}} = 40$ and 150 km s^{-1}. The model colours become redder until the white dwarfs become cool enough to show infrared absorption due to molecular hydrogen (Hansen 1998). We selected targets for follow-up spectroscopy and near-infrared photometry based on their reduced proper motion and colours. To find the elusive halo white dwarfs and other white dwarfs with high tangential velocities, we targeted objects with $H_{\mathrm{g}} > 21$ mag and below the $V_{\mathrm{tan}} = 40$ km s^{-1} line.

2.2 Optical spectroscopy

We obtained follow-up optical spectroscopy of 32 white dwarf candidates at the 6.5-m Multiple Mirror Telescope (MMT) equipped with the Blue Channel Spectrograph (Schmidt, Weymann & Foltz 1989) on UT 2009 June 18–23 and 2009 November 19–20. We used a 1.25-arcsec slit and the 500 line mm^{-1} grating in first order to obtain spectra over the range 3660–6800 Å and with a resolving power
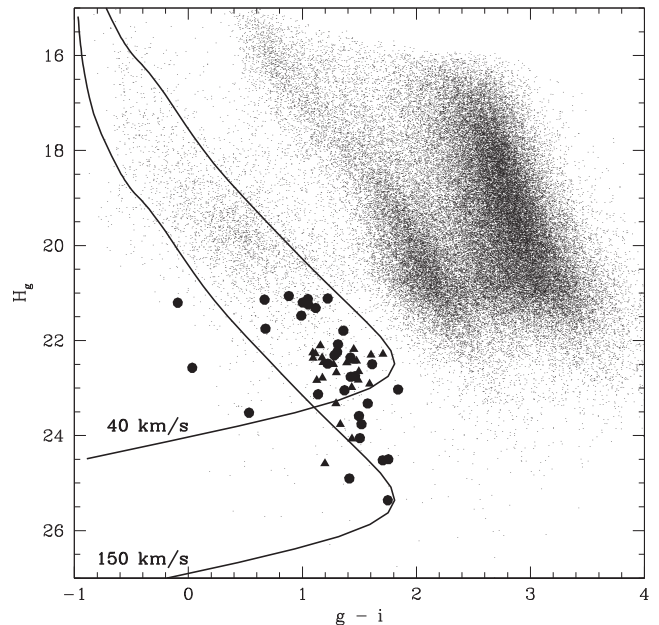
Figure 1. The reduced proper motion diagram for a portion of the Munn et al. (2014) proper motion survey. White dwarf evolutionary tracks for tangential velocities of 40 and 150 km s^{-1} are shown as solid lines. Filled circles mark spectroscopically confirmed white dwarfs with $H_{\mathrm{g}} > 21$ mag and triangles show our targets with SWIRC near-infrared photometry, but with no follow-up spectroscopy.

of $R = 1200$. We obtained all spectra at the parallactic angle and acquired He–Ar–Ne comparison lamp exposures for wavelength calibration. We use observations of the cool white dwarf G24-9 for flux calibration.

Out of the 32 candidates with spectra, only two (SDSS J024416.07−090919.7 and J172431.61+261543.1) are metal-poor halo subdwarfs. The remaining objects are confirmed to be DA, DC, or DZ white dwarfs. This relatively small (2 out of 32) contamination rate from subdwarfs demonstrates that our white dwarf sample is relatively clean.

Fig. 2 shows the spectra for the five DA white dwarfs in our sample. Two of the DAs, J1513+4743 and J1624+4156, are warm enough ($T_{\mathrm{eff}} \approx 5900$ K) to show Hα and a few of the higher order Balmer lines, while the remaining three DAs only show Hα, which implies effective temperatures near 5000 K.

Fig. 3 shows the MMT spectra for the 24 DC white dwarfs in our sample, including the three cool DCs presented in Kilic et al. (2010a). All of these 24 targets have featureless spectra that are rising towards the infrared, indicating temperatures below 5000 K.

2.3 Near-infrared photometry

We obtained *J*- and *H*-band imaging observations of 40 of our targets using the Smithsonian Widefield Infrared Camera (SWIRC; Brown et al. 2008) on the MMT on UT 2011 March 23–24. SWIRC has a 5.12×5.12 arcmin^2 field of view at a resolution of 0.15 arcsec pixel^{-1}. We observed each target on a dozen or more dither positions, and obtained dark frames and sky flats each evening. We used the SWIRC data reduction pipeline to perform dark correction, flat-fielding, and sky subtraction, and to produce a combined image for each field in each filter. We use the Two Micron All Sky Survey
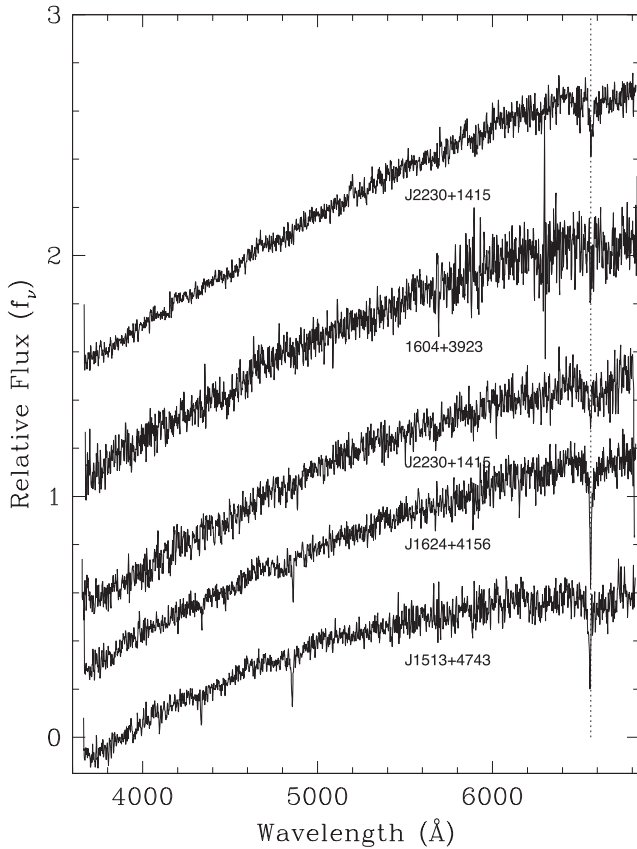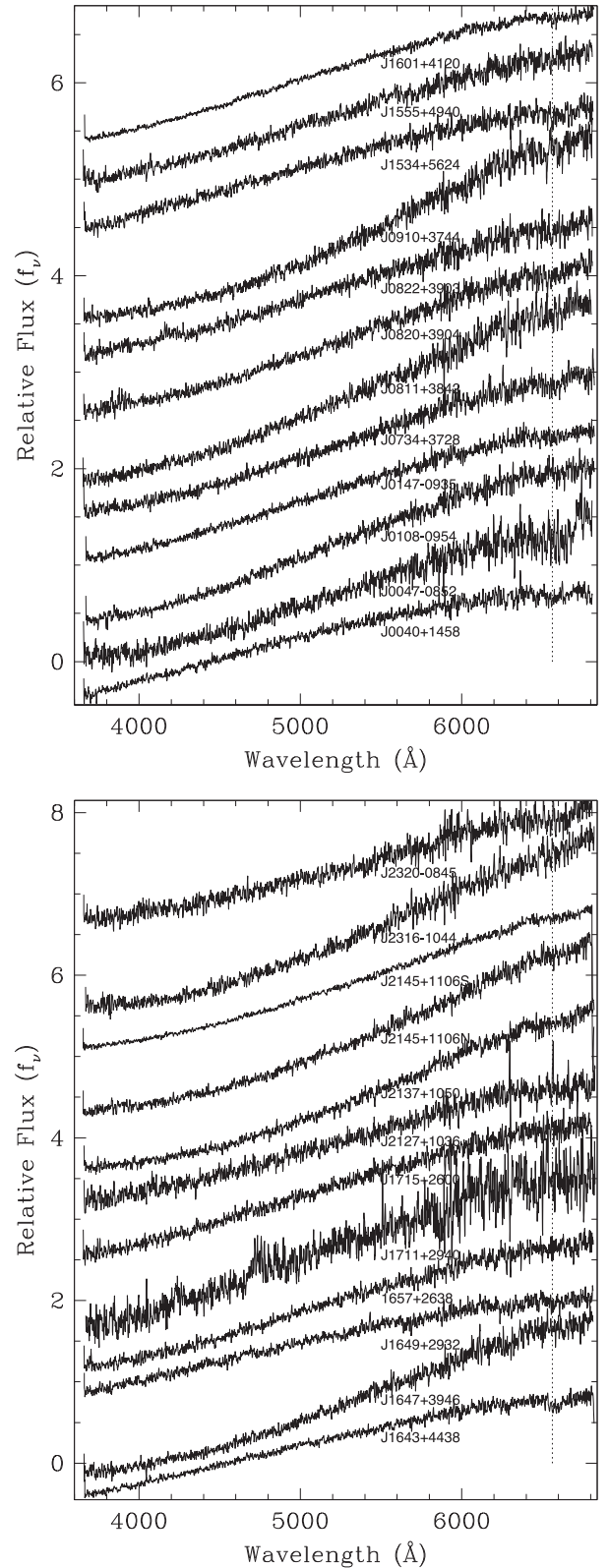
Figure 2. Optical spectra for the five DA white dwarfs in our sample. The dotted line marks Hα.

Figure 3. Optical spectra for 24 DC white dwarfs in our sample.

(2MASS) stars in the SWIRC field of view for photometric and astrometric calibration. In addition, near-infrared photometry for two more targets, J0040+1458 and J1649+2932, are available from the UKIRT Infrared Deep Sky Survey (UKIDSS; Lawrence et al. 2007) Large Area Survey. Table 1 presents the *ugriz* and *JH* photometry for our sample of 57 targets with follow-up spectroscopy and/or near-infrared photometry.

Fig. 4 presents optical and infrared colour–colour diagrams for the same stars, along with the predicted colours of pure H and pure He atmosphere white dwarfs. The differences between these models are relatively minor in the optical colour–colour diagrams, except for the ultracool white dwarfs with $T_{\rm eff} < 4000$ K. The pure H models predict the colours to get redder until the onset of the collision-induced absorption (CIA) due to molecular hydrogen, which leads to a blue hook feature. This transition occurs at 3750 K for the $r - i$ colour, whereas it occurs at 4500 K for the $r - H$ colour. The colours for our sample of 57 stars, including the targets with and without follow-up spectroscopy, are consistent with the white dwarf model colours within the errors. The majority of the targets with $g - r \geq 1.0$ mag ($T_{\rm eff} \leq 4250$ K) show bluer $r - H$ colours than the pure He model sequence, indicating that the coolest white dwarfs in our sample have H-rich atmospheres.

We use the SWIRC astrometry to verify the proper motion measurements from our optical imaging survey. Given the relatively small field of view of the SWIRC camera and the limited number of 2MASS stars available in each field, the astrometric precision is significantly worse in the SWIRC images compared to the Bok 90-inch and USNO 1.3-m optical data. We find

that the proper motion measurements from the SWIRC data are on average 54 ± 44 mas yr^{-1} higher. Nevertheless, all but one of our targets, J1513+4743, have SWIRC-SDSS proper motion measurements consistent with the proper motion measurements

Table 1. Optical and near-infrared photometry of white dwarf candidates.

SDSS	u	g	r	i	z	J	H
J213730.86+105041.5	23.30 ± 0.54	21.77 ± 0.06	20.51 ± 0.03	20.01 ± 0.03	19.73 ± 0.08	19.21 ± 0.10	19.25 ± 0.18
J214538.16+110626.6	23.72 ± 0.52	21.49 ± 0.04	20.22 ± 0.02	19.77 ± 0.02	19.61 ± 0.05	18.87 ± 0.07	19.00 ± 0.10
J214538.60+110619.1	23.47 ± 0.45	21.01 ± 0.03	19.93 ± 0.02	19.49 ± 0.02	19.29 ± 0.04	18.54 ± 0.06	19.31 ± 0.06
J004022.47+145835.0	22.23 ± 0.23	20.56 ± 0.03	19.83 ± 0.02	19.53 ± 0.03	19.43 ± 0.06	18.60 ± 0.10	18.39 ± 0.12
J004725.61−085223.9	25.78 ± 0.74	21.65 ± 0.06	20.67 ± 0.04	20.29 ± 0.05	20.17 ± 0.15	. . .	. . .
J010838.42−095415.7	24.07 ± 1.04	21.56 ± 0.06	20.61 ± 0.04	20.20 ± 0.04	19.98 ± 0.13	. . .	. . .
J014749.07−093537.4	22.98 ± 0.53	21.64 ± 0.07	20.70 ± 0.04	20.44 ± 0.05	20.39 ± 0.24	. . .	. . .
J073417.76+372842.6	24.01 ± 0.74	21.88 ± 0.07	20.95 ± 0.05	20.57 ± 0.04	20.44 ± 0.14	19.59 ± 0.09	20.08 ± 0.17
J074942.95+294716.7	22.45 ± 0.26	20.80 ± 0.03	19.95 ± 0.02	19.64 ± 0.03	19.49 ± 0.06	18.56 ± 0.04	18.37 ± 0.05
J080505.26+273557.2	23.73 ± 0.62	21.52 ± 0.06	20.59 ± 0.03	20.25 ± 0.03	20.28 ± 0.12	19.05 ± 0.06	19.16 ± 0.06
J080545.80+374720.4	23.87 ± 0.64	21.12 ± 0.04	20.39 ± 0.03	20.08 ± 0.03	19.87 ± 0.10	19.13 ± 0.05	18.86 ± 0.06
J081140.07+384202.2	23.87 ± 0.69	21.89 ± 0.07	20.84 ± 0.04	20.55 ± 0.04	20.30 ± 0.11	19.50 ± 0.06	19.24 ± 0.08
J081735.51+310625.5	22.39 ± 0.23	20.52 ± 0.03	19.50 ± 0.02	19.14 ± 0.02	18.89 ± 0.03	18.14 ± 0.03	17.84 ± 0.04
J082035.23+390419.9	22.72 ± 0.32	22.01 ± 0.07	20.86 ± 0.04	20.53 ± 0.04	20.29 ± 0.09	19.31 ± 0.05	19.49 ± 0.10
J082255.41+390302.7	23.16 ± 0.34	21.87 ± 0.05	20.90 ± 0.04	20.49 ± 0.03	20.37 ± 0.11	19.19 ± 0.06	19.24 ± 0.08
J082842.31+352729.5	21.43 ± 0.09	19.84 ± 0.02	19.06 ± 0.02	18.73 ± 0.02	18.69 ± 0.03	17.88 ± 0.03	17.47 ± 0.04
J084802.30+420429.7	22.92 ± 0.37	21.72 ± 0.06	20.79 ± 0.04	20.53 ± 0.05	20.41 ± 0.14	19.63 ± 0.06	19.29 ± 0.08
J085441.14+390700.1	22.87 ± 0.28	21.22 ± 0.03	20.40 ± 0.03	20.12 ± 0.03	20.03 ± 0.08	19.17 ± 0.04	18.83 ± 0.06
J091035.82+374454.8	23.85 ± 0.63	21.79 ± 0.06	20.53 ± 0.03	19.95 ± 0.03	19.64 ± 0.07	18.95 ± 0.04	18.80 ± 0.05
J091823.08+502826.4	22.60 ± 0.26	20.72 ± 0.03	19.87 ± 0.02	19.62 ± 0.02	19.47 ± 0.06	18.67 ± 0.04	18.38 ± 0.04
J092716.99+485233.3	22.96 ± 0.30	20.65 ± 0.02	19.59 ± 0.02	19.17 ± 0.03	19.11 ± 0.05	19.12 ± 0.06	19.60 ± 0.14
J100953.03+534732.9	23.82 ± 0.84	21.82 ± 0.07	20.75 ± 0.04	20.40 ± 0.04	19.86 ± 0.10	19.09 ± 0.06	18.92 ± 0.07
J102417.17+492011.3	22.83 ± 0.29	21.59 ± 0.06	20.70 ± 0.03	20.42 ± 0.04	20.15 ± 0.10	19.46 ± 0.08	18.89 ± 0.07
J105652.84+504321.3	23.56 ± 0.56	21.40 ± 0.04	20.37 ± 0.03	19.99 ± 0.03	19.79 ± 0.08	19.05 ± 0.04	18.78 ± 0.05
J110105.01+485437.9	23.00 ± 0.51	20.88 ± 0.04	19.92 ± 0.05	19.68 ± 0.03	19.67 ± 0.09	18.75 ± 0.04	18.50 ± 0.05
J114558.52+563806.8	23.08 ± 0.52	21.73 ± 0.06	20.93 ± 0.06	20.62 ± 0.06	20.26 ± 0.15	19.64 ± 0.08	19.35 ± 0.07
J120514.49+550217.2	22.84 ± 0.43	21.31 ± 0.04	20.37 ± 0.03	20.00 ± 0.03	19.88 ± 0.10	18.94 ± 0.05	18.68 ± 0.04
J132358.81+022342.2	23.10 ± 0.46	21.88 ± 0.07	20.91 ± 0.04	20.60 ± 0.05	20.52 ± 0.16	19.43 ± 0.07	19.37 ± 0.07
J133309.98+494227.2	24.03 ± 0.78	21.15 ± 0.04	20.23 ± 0.03	19.86 ± 0.04	19.60 ± 0.06	18.79 ± 0.04	18.60 ± 0.04
J140907.89−010036.9	22.94 ± 0.28	21.64 ± 0.06	20.58 ± 0.03	20.18 ± 0.03	19.97 ± 0.10	19.12 ± 0.06	19.06 ± 0.06
J142136.69+035612.4	24.39 ± 0.97	21.89 ± 0.08	20.82 ± 0.05	20.43 ± 0.04	20.23 ± 0.16	19.19 ± 0.06	19.04 ± 0.07
J143400.55+534525.2	22.95 ± 0.44	21.20 ± 0.04	20.28 ± 0.03	19.89 ± 0.03	19.62 ± 0.07	18.99 ± 0.04	18.64 ± 0.06
J144417.48+602555.1	23.73 ± 0.61	21.62 ± 0.05	20.65 ± 0.03	20.42 ± 0.04	20.52 ± 0.13	19.50 ± 0.07	19.09 ± 0.10
J144606.46+025811.5	23.70 ± 0.85	21.72 ± 0.12	20.64 ± 0.07	20.33 ± 0.06	30.02 ± 0.12	19.03 ± 0.06	18.92 ± 0.09
J150904.50+540825.2	24.60 ± 1.03	21.97 ± 0.08	20.94 ± 0.05	20.49 ± 0.05	20.17 ± 0.13	19.31 ± 0.07	19.13 ± 0.08
J151319.26+502318.6	23.39 ± 0.44	21.96 ± 0.07	20.70 ± 0.03	20.30 ± 0.03	19.93 ± 0.07	18.85 ± 0.05	19.30 ± 0.08
J151321.20+474324.2	20.82 ± 0.06	19.92 ± 0.03	19.63 ± 0.02	19.42 ± 0.02	19.41 ± 0.06	18.62 ± 0.05	18.55 ± 0.21
J151555.53+593045.3	25.19 ± 0.86	21.96 ± 0.06	20.78 ± 0.03	20.34 ± 0.04	20.24 ± 0.09	19.40 ± 0.08	19.66 ± 0.10
J153300.94−001212.2	23.65 ± 0.59	22.05 ± 0.07	20.89 ± 0.04	20.46 ± 0.04	20.16 ± 0.12	19.24 ± 0.07	19.07 ± 0.09
J153432.25+562455.7	21.76 ± 0.14	20.26 ± 0.02	19.62 ± 0.02	19.36 ± 0.03	19.28 ± 0.05	. . .	. . .
J155243.40+463819.4	21.53 ± 0.11	20.09 ± 0.02	19.50 ± 0.02	19.31 ± 0.02	19.28 ± 0.05	. . .	. . .
J155501.57+494056.4	25.76 ± 0.64	21.84 ± 0.08	20.77 ± 0.04	20.46 ± 0.05	20.30 ± 0.16	19.29 ± 0.07	19.23 ± 0.07
J160125.48+412014.1	21.20 ± 0.07	19.28 ± 0.02	18.44 ± 0.02	18.15 ± 0.02	18.08 ± 0.02	. . .	. . .
J160130.82+420427.6	24.19 ± 0.98	21.65 ± 0.06	20.71 ± 0.04	20.37 ± 0.04	20.37 ± 0.17	19.29 ± 0.07	19.01 ± 0.09
J160424.38+392330.5	21.88 ± 0.20	20.51 ± 0.03	19.87 ± 0.02	19.67 ± 0.03	19.44 ± 0.07	. . .	. . .
J162417.93+415656.6	21.21 ± 0.09	20.18 ± 0.02	19.84 ± 0.02	19.69 ± 0.03	19.62 ± 0.07	. . .	. . .
J162724.57+372643.1	21.78 ± 0.10	19.80 ± 0.02	18.94 ± 0.02	18.64 ± 0.01	18.53 ± 0.03	17.60 ± 0.03	17.39 ± 0.03
J164358.79+443855.4	21.42 ± 0.10	19.84 ± 0.02	19.11 ± 0.02	18.88 ± 0.01	18.81 ± 0.04	17.91 ± 0.03	17.63 ± 0.03
J164745.45+394638.6	24.56 ± 1.09	21.55 ± 0.05	20.30 ± 0.03	19.89 ± 0.03	19.84 ± 0.08	18.91 ± 0.05	18.60 ± 0.05
J164931.91+293247.7	22.19 ± 0.15	20.61 ± 0.03	19.90 ± 0.02	19.63 ± 0.02	19.51 ± 0.08	18.62 ± 0.06	18.52 ± 0.11
J165723.84+263843.5	24.80 ± 0.80	21.33 ± 0.04	20.28 ± 0.03	19.99 ± 0.03	19.77 ± 0.10	19.24 ± 0.08	19.20 ± 0.10
J171135.27+294046.0	23.00 ± 0.33	21.11 ± 0.03	20.37 ± 0.03	19.96 ± 0.02	19.85 ± 0.07	18.73 ± 0.05	18.41 ± 0.07
J171543.76+260016.9	22.82 ± 0.40	21.25 ± 0.04	20.45 ± 0.03	20.06 ± 0.03	19.91 ± 0.10	18.81 ± 0.07	18.27 ± 0.04
J212739.00+103655.1	22.77 ± 0.41	21.67 ± 0.06	20.71 ± 0.04	20.35 ± 0.04	20.11 ± 0.13	. . .	. . .
J223038.21+141505.7	21.86 ± 0.15	20.37 ± 0.03	19.87 ± 0.02	19.64 ± 0.02	19.60 ± 0.07	. . .	. . .
J231617.67−104411.0	23.41 ± 0.67	21.98 ± 0.09	20.99 ± 0.05	20.56 ± 0.05	20.34 ± 0.14	. . .	. . .
J232018.23−084516.7	25.55 ± 0.95	21.63 ± 0.07	20.57 ± 0.04	20.20 ± 0.05	19.97 ± 0.15	. . .	. . .
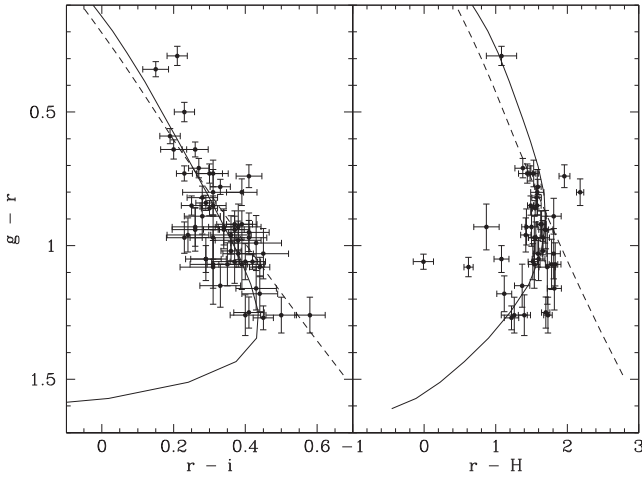
Figure 4. Colour–colour diagrams for our sample of 57 white dwarf candidates. Solid and dashed lines show the predicted colours for pure H ($T_{eff} \geq$ 2500 K) and pure He atmosphere ($T_{eff} \geq$ 3500 K) white dwarfs with log g = 8 (Bergeron, Saumon & Wesemael 1995), respectively.

from our optical data within 3σ. J1513+4743 is spectroscopically confirmed to be a DA white dwarf. Hence, the contamination rate of our sample of 57 stars by objects with incorrectly measured proper motions should be relatively small.

3 PHOTOMETRIC ANALYSIS

3.1 Model atmospheres

Our model atmospheres come from the local thermodynamic equilibrium (LTE) model atmosphere code described in Bergeron et al. (1995) and references within, along with the recent improvements in the calculations for the Stark broadening of hydrogen lines discussed in Tremblay & Bergeron (2009). We follow the method of Holberg & Bergeron (2006) and convert the observed magnitudes into fluxes, and use a non-linear least-squares method to fit the resulting SEDs to predictions from model atmospheres. Given that all our targets appear to be within 150 pc, we do not correct for extinction. We consider only the temperature and the solid angle $\pi(R/D)^2$, where R is the radius of the white dwarf and D is its distance from the Earth, as free parameters. Convection is modelled by the ML/α = 0.7 prescription of mixing length theory. For a more detailed discussion of our fitting technique, see Bergeron, Leggett & Ruiz (2001); for details of our helium-atmosphere models, see Bergeron et al. (2011). Since we do not have parallax measurements for our objects, we assume a surface gravity of log g = 8. This is appropriate, as the white dwarf mass distribution in the solar neighbourhood peaks at about 0.6 M$_\odot$ (Tremblay et al. 2013). We discuss the effects of this choice in Section 4.

Below about 5000 K, Hα is not visible. However, the presence of hydrogen can still be seen in the blue from the red wing of Lyα absorption (Kowalski & Saumon 2006), and in the infrared from CIA due to molecular hydrogen. Cool white dwarfs with pure helium atmospheres are not subject to these opacities, so their SEDs should appear similar to a blackbody. Because of this, atmospheric composition can still be determined from ultraviolet and near-infrared data. Table 2 presents the best-fitting atmospheric compositions, temperatures, distances, and cooling ages for our targets, as well as

their proper motions and tangential velocities. Below, we discuss the pure H, pure He, and mixed H/He atmosphere targets separately, and highlight the most interesting objects in the sample.

3.2 Pure H solutions

Of our 57 targets, only 45 have the near-infrared data that are needed to observe the CIA that allows us to detect the presence of hydrogen. Of these 45 objects, 12 have SEDs best fit by pure hydrogen models. Fig. 5 shows the SEDs and our model fits for four of these objects (full sample is available online). We show the photometric data as error bars and the best-fitting model fluxes for pure H and pure He composition as filled and open circles, respectively.

J1513+4743 is the only DA white dwarf in our sample with near-infrared photometry available (the four other DAs are discussed in Section 3.5), and the pure H model is a better fit to the SED than the pure He model. For the remaining objects, we chose the composition based on the solution that best fits the SED. Our sample includes three previously published H-atmosphere DC white dwarfs: J2137+1050, J2145+1106N, and J2145+1106S (Kilic et al. 2010a). Our temperature estimates of 3670 ± 160, 3720 ± 110, and 3960 ± 100 K, respectively, agree with the previously published values of 3780, 3730, and 4110 K (Kilic et al. 2010a) within the errors.

With the exception of the DA WD J1513+4743, all of the remaining 11 objects that are best explained by pure H atmosphere models have $T_{eff} \leq$ 4250 K. These objects appear significantly fainter in the H band than expected from the blackbody-like SEDs of pure He atmosphere white dwarfs, indicating that they have H-rich atmospheres. In addition to the previously published J2137+1050 and J2145+1106N (Kilic et al. 2010a), we identify three new white dwarfs with $T_{eff} \leq$ 3700 K; namely J0734+3728, J1515+5930, and J1657+2638. The latter is the coolest white dwarf known (T_{eff} = 3550 ± 100 K) with an SED that is matched relatively well by a pure H atmosphere model. The implied cooling age for such a cool white dwarf is 10.1 Gyr assuming an average mass, log g = 8, white dwarf.

3.3 Pure He solutions

For our remaining 33 objects with infrared data, 29 show no evidence of CIA and are best fit by pure He atmosphere models. Fig. 6 shows the SEDs for a sample of these targets. All 29 of these objects have T_{eff} in the range 4240–4930 K. Nine stars have optical spectra available, and all nine are DC white dwarfs.

The differences between the pure H and pure He model fits are relatively small in this temperature range, and additional K-band photometry would be useful to confirm the atmospheric composition for these stars. However, Bergeron (2001) and Kilic et al. (2010b) also find an overabundance of pure He atmosphere white dwarfs in the temperature range 4500–5000 K. Kilic et al. (2010b) discuss a few potential problems that could lead to misclassification of spectral types for these stars, including problems with the CIA calculations, or small shifts in the *ugriz* or *JH* photometric calibration.

3.4 Mixed atmosphere solutions

The last four targets with infrared data (J0910+3744, J0927+4852, J1513+4743, and J1555+4940) have SEDs that are inconsistent with either a pure H or pure He atmosphere solution. We fit the SEDs

Table 2. Physical parameters of our white dwarf sample. Source of the optical spectroscopic observations: 1 – this paper; 2 – Kilic et al. (2010b); and 3 – Kilic et al. (2010a).

| Object (SDSS)	Spectral type	Source	Composition (log He/H)	$T_{\rm eff}$ (K)	d (pc)	Cooling age (Gyr)	$\mu_{\rm RA}$ (mas yr^{-1})	$\mu_{\rm Dec.}$ (mas yr^{-1})	$V_{\rm tan}$ (km s^{-1})
J2137+1050	DC	2	H	3670 ± 160	75	9.8	-228.9	-473.6	187.1
J2145+1106N	DC	2	H	3720 ± 110	68	9.7	191.9	-366.9	134.4
J2145+1106S	DC	2	H	3960 ± 100	65	9.1	185.9	-367.7	126.5
J0040+1458	DC	1	He	4890 ± 90	94	6.3	128.1	18.5	57.6
J0047−0852	DC	1	H	3140 ± 160	68	11.0	211	-27.2	69.0
			He	3920 ± 120	79	8.5			79.2
J0108−0954	DC	1	H	3630 ± 520	77	9.9	-70.1	-183.9	72.1
			He	4360 ± 150	100	7.5			93.6
J0147−0935	DC	1	H	4300 ± 320	108	8.2	211.5	-26.4	109.0
			He	4640 ± 190	126	6.9			127.3
J0734+3728	DC	1	H	3700 ± 140	94	9.8	-3.5	-114	50.5
J0749+2947	...	...	He	4690 ± 60	90	6.7	216.1	-133.9	108.9
J0805+2735	...	...	H	4130 ± 120	94	8.7	68.1	-215.9	101.1
J0805+3747	...	...	He	4820 ± 80	118	6.4	-91.8	-135.5	91.4
J0811+3842	DC	1	He	4570 ± 110	131	7.0	99.3	-147.4	110.1
J0817+3106	...	...	He	4510 ± 50	67	7.1	231.4	-93.8	79.8
J0820+3904	DC	1	H	4050 ± 150	104	8.9	-172	-129	106.0
J0822+3903	DC	1	H	4190 ± 150	109	8.5	274.2	-316.5	216.5
J0828+3527	DC	3	He	4840 ± 60	65	6.4	-13.1	-161	49.9
J0848+4204	...	...	He	4820 ± 120	146	6.4	-137.8	-32.5	97.9
J0854+3907	...	...	He	4810 ± 80	119	6.5	-29.9	-162.1	93.2
J0910+3744	DC	1	-3.69	3450 ± 190	63	9.5	-143.6	-91.7	50.7
J0918+5028	...	...	He	4810 ± 70	94	6.5	-108.2	-185.9	96.3
J0927+4852	...	...	6.33	3210 ± 90	42	9.9	216.5	-70.1	45.4
J1009+5347	...	...	He	4290 ± 100	104	7.7	-120.1	-254.3	138.2
J1024+4920	...	...	He	4680 ± 120	128	6.8	-80.1	-391.8	242.1
J1056+5043	...	...	He	4560 ± 70	104	7.0	-36.7	-119.7	61.7
J1101+4854	...	...	He	4770 ± 80	97	6.6	73.9	-196.1	96.8
J1145+5638	...	...	He	4780 ± 120	148	6.5	-127	-114.3	119.8
J1205+5502	...	...	He	4560 ± 70	102	7.0	-23.4	-311.8	151.2
J1323+0223	...	...	H	4250 ± 170	116	8.4	-112.2	-50.6	67.5
J1333+4942	...	...	He	4550 ± 60	95	7.0	-174.7	-0.9	79.0
J1409−0100	...	...	H	4090 ± 120	92	8.8	-125.2	75.8	63.7
J1421+0356	...	...	He	4340 ± 100	111	7.5	-156.2	-15	82.3
J1434+5345	...	...	He	4600 ± 70	100	7.0	-143	136.6	93.5
J1444+6025	...	...	He	4730 ± 100	132	6.6	-18.1	-134.3	85.1
J1446+0258	...	...	He	4360 ± 140	104	7.5	-196.2	43.2	99.5
J1509+5408	...	...	He	4320 ± 110	114	7.6	13.3	-135.7	73.9
J1513+5023	...	...	-3.22	3860 ± 180	86	8.7	-98.6	-49.4	45.0
J1513+4743	DA	1	H	5960 ± 120	124	2.3	-500.8	-147.1	305.9
J1515+5930	...	...	H	3700 ± 120	87	9.8	-74.6	90.4	48.5
J1533−0012	...	...	He	4240 ± 100	107	7.8	-44.2	-140.2	74.7
J1534+5624	DC	1	H	4900 ± 120	84	6.2	-140.3	119.5	73.2
			He	5050^{+120}_{-70}	93	5.7			81.0
J1552+4638	DA	1	H	5100^{+120}_{-100}	88	5.2	-48.7	-181.5	78.1
J1555+4940	DC	1	-3.16	3910 ± 180	94	8.5	27.1	-127.1	57.6
J1601+4120	DC	1	H	4080 ± 120	36	8.8	74.8	-228.7	40.6
			He	4610 ± 60	44	6.9			50.5
J1601+4204	...	...	He	4540 ± 110	119	7.1	-111.1	70.9	74.1
J1604+3923	DA	1	H	5010 ± 140	99	5.6	15.3	-152.1	72.0
J1624+4156	DA	1	H	5840 ± 150	133	2.4	27.7	-194.1	123.6
J1627+3726	DC	3	He	4650 ± 50	57	6.8	-24.1	-169.3	46.0
J1643+4438	DC	1	He	4910^{+60}_{-40}	70	6.2	42.8	-197.7	66.8
J1647+3946	DC	1	He	4360 ± 70	91	7.5	-114.3	-111.8	69.3
J1649+2932	DC	1	He	4930 ± 80	99	6.2	121.3	16.1	57.6
J1657+2638	DC	1	H	3550 ± 100	67	10.1	-73.3	-104.6	40.3
J1711+2940	DC	1	He	4550 ± 70	97	7.1	57.7	-165.8	80.7
J1715+2600	DC	1	He	4310 ± 80	88	7.6	-34.3	-162.2	69.5
J2127+1036	DC	1	H	3970 ± 370	93	9.1	-112.5	-65.9	57.5
			He	4470 ± 160	113	7.2			69.7
J2230+1415	DA	1	H	5210 ± 140	107	4.6	-18.3	-142.3	72.7
J2316−1044	DC	1	H	3670 ± 790	93	9.8	237.7	-72	109.7
			He	4310 ± 200	115	7.6			136.0
J2320−0845	DC	1	H	3240 ± 190	67	10.8	166.7	20.3	53.3
			He	4010 ± 130	80	8.3			63.7
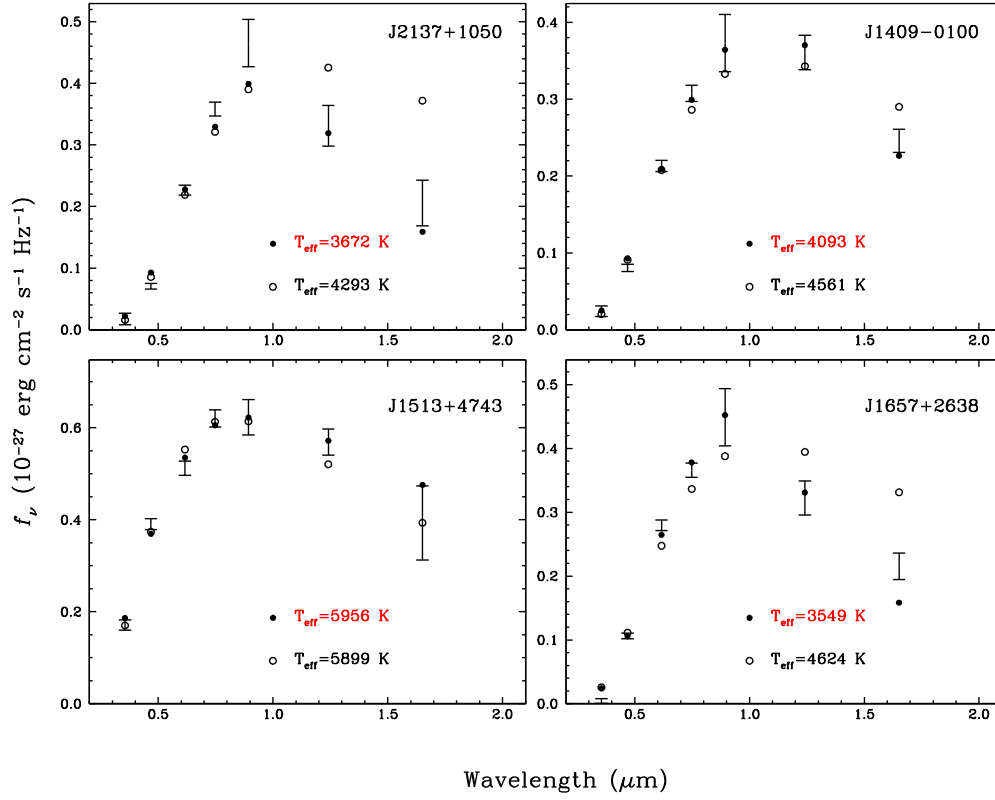
Figure 5. Fits to the SEDs for four of our white dwarfs with pure H atmospheres (full sample available online). Filled circles are pure H models, and open circles are pure He models (included for comparison).
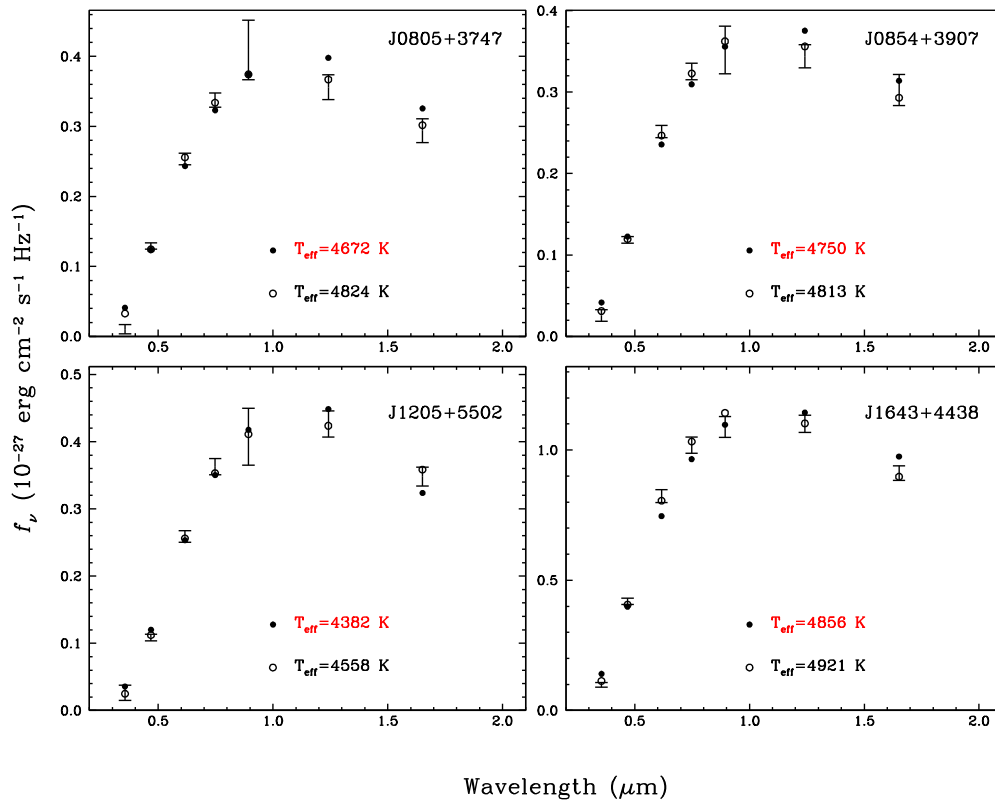
Figure 6. Fits to the SEDs for four of our white dwarfs with pure He atmospheres (full sample available online). Filled circles are pure H models (included for comparison), and open circles are pure He models.
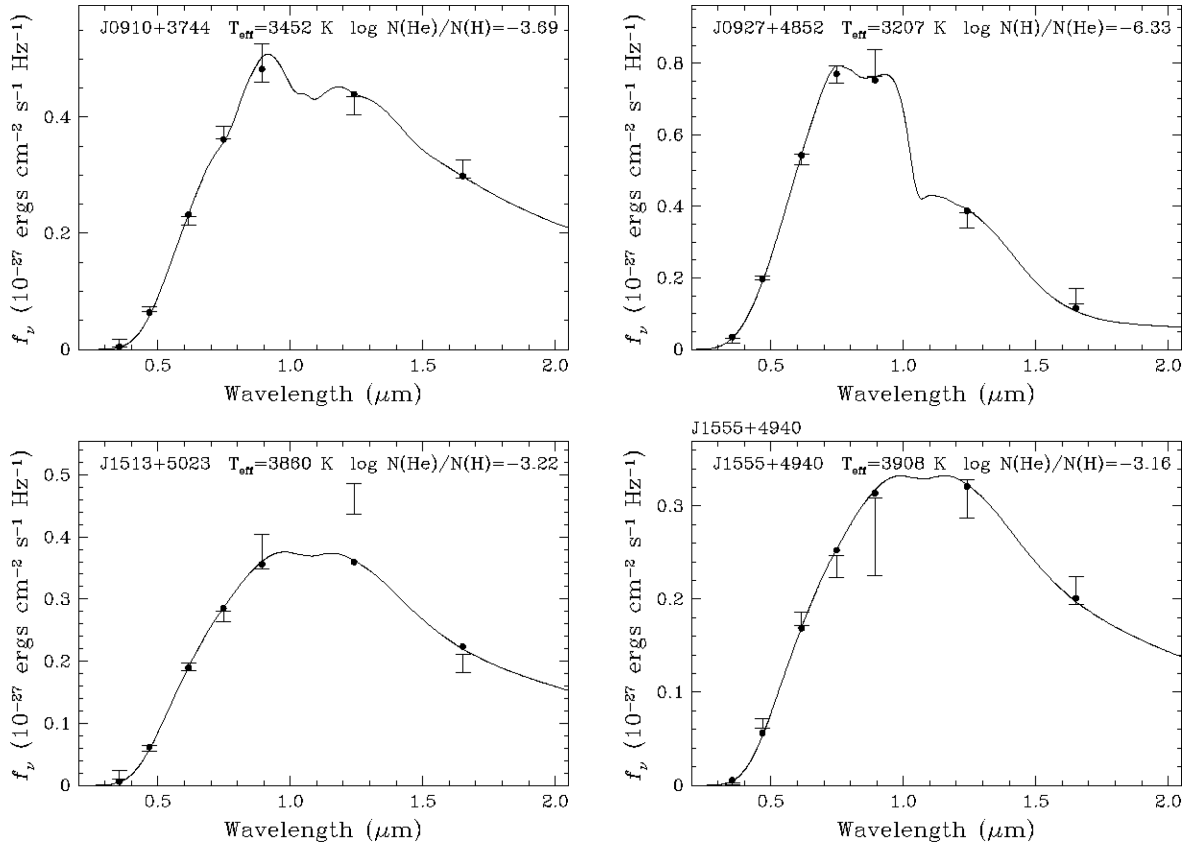
Figure 7. Fits to the SEDs of the four white dwarfs best fit by mixed atmosphere models.

of these stars with a mixed H/He atmosphere model. The mixed models allow for significant H_2–He CIA at higher temperatures than seen for H_2–H_2, as CIA becomes an effective opacity source at higher temperatures in cool He-rich white dwarfs due to lower opacities and higher atmospheric pressures (Bergeron & Leggett 2002).

Fig. 7 shows our mixed H/He atmosphere model fits for these four objects. The models yield $\log (\text{He/H})$ of $-3.7, 6.3, -3.2$, and -3.2 and temperatures of 3450, 3210, 3860, and 3910 K, respectively. Note that these models predict CIA absorption features around 0.8 and 1.1 μm that are never observed in cool white dwarfs. Hence, the temperature and composition estimates for such infrared-faint stars are problematic (see the discussion in Kilic et al. 2010b; Gianninas et al. 2015).

The coolest object among these four stars, J0927+4852 appears to be similar to WD 0346+246. Oppenheimer et al. (2001) originally found a $T_{\text{eff}} = 3750$ K and $\log (\text{He/H}) = 6.4$ for WD 0346+246, for an assumed surface gravity of $\log g = 8$. However, Bergeron (2001) showed that such a He-rich atmosphere would require accretion rates from the interstellar medium too low to be realistic. With the addition of parallax observations to constrain the distance, they estimated a more realistic solution with $T_{\text{eff}} = 3780$ K, $\log (\text{He/H}) = 1.3$, and $\log g = 8.34$. A reanalysis by Kilic et al. (2012) that include the red wing of the Lyα opacity indicate a similar solution with $T_{\text{eff}} = 3650$ K, $\log (\text{He/H}) = -0.4$, and $\log g = 8.3$. Adopting a similar $\log g$ value for J0927+4852 would yield a T_{eff} of 3730 K and $\log (\text{He/H})$ of 0.3.

This exercise shows the problems with constraining the atmospheric composition of ultracool white dwarfs, and the need for parallax observations to derive accurate parameters for such white dwarfs. Regardless of these issues, all four mixed atmosphere white dwarfs appear to be ultracool ($T_{\text{eff}} < 4000$ K), bringing the total number of ultracool white dwarfs in our sample to 10.

3.5 Targets without infrared data

There are 12 spectroscopically confirmed white dwarfs in our sample that lack infrared photometry. Fig. 8 displays the SEDs along with the pure H and pure He model fits for a subsample of these objects. The spectra of four of these objects: J1552+4638, J1604+3923, J1624+4156, and J2230+1415 confirm that they are DA white dwarfs, and the pure H models reproduce the SEDs and spectra reasonably well. This brings our final number of pure H solutions to 16 stars.

The remaining eight objects without infrared data are confirmed to be DC white dwarfs. For the most part, the pure H and pure He models are nearly indistinguishable in the optical for these objects and we cannot determine their composition. Table 2 shows the results for both pure H and pure He solutions for these objects.

All of these targets have SEDs rising towards 1 μm, hence the lack of infrared data limits the precision of these temperature measurements. However, given the lack of He atmosphere white dwarfs below 4240 K, we do not expect J0047−0852 and J2320−0845 to
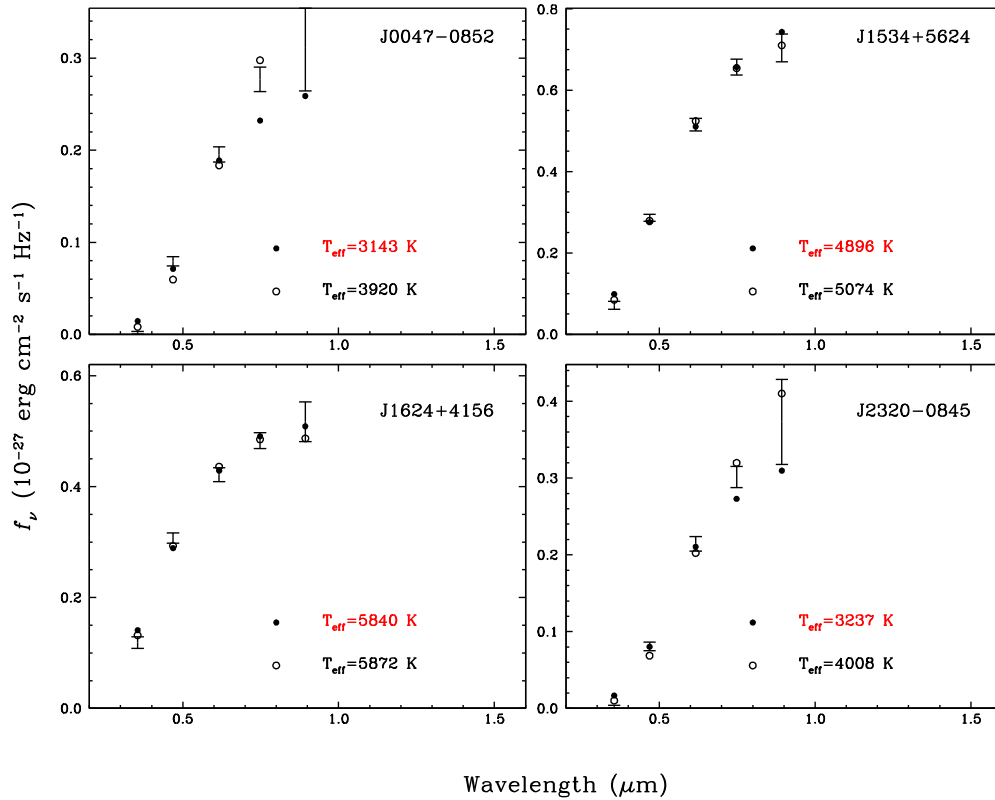
Figure 8. Fits to the SEDs for a sample of our white dwarf lacking infrared data (full sample available online). Filled circles are pure H models, and open circles are pure He models. As can be seen, no model is clearly better.

have pure He atmospheres, and if they were to have pure H atmospheres, they would be the coolest white dwarfs in our sample, with T_{eff} of 3140 ± 160 and 3240 ± 190 K, respectively. J0108−0954, J2127+1036, and J2316−1044 are also potentially ultracool objects if the pure H solution is correct, which would bring the total number of ultracool white dwarf candidates in our sample to 15. Without infrared data, however, we cannot rule out the pure He solution, or the possibility of a mixed H/He atmosphere for J0047−0852 and J2320−0845.

4 KINEMATIC MEMBERSHIP

The estimated temperatures for our targets yield white dwarf cooling ages between 5 and 10 Gyr, with the only notable exceptions being J1513+4743 and J1624+4156, which have cooling ages of 2.3 and 2.4 Gyr, respectively. Eight objects have cooling ages longer than 9 Gyr, with the oldest being J1657+2638 at 10.1 Gyr. However, in order to associate a white dwarf with the thick disc or halo, it is important to determine the total stellar age (Bergeron et al. 2005). The main-sequence lifetime of the $\approx 2\,M_\odot$ progenitor of a $0.6\,M_\odot$ white dwarf is 1.0–1.3 Gyr; therefore, the total ages of our objects on average range from 6 to 11 Gyr, with J1513+4743 and J1624+4156 having total ages between 3.3 and 3.7 Gyr.

Fig. 9 shows U versus V (bottom) and W versus V (top) velocities of our objects (assuming a radial velocity of 0 km s^{-1} and calculated using the prescription of Johnson & Soderblom 1987), as well as the 3σ ellipsoids of the halo, thick disc, and thin disc

populations (Chiba & Beers 2000). The filled, open, and red circles represent the objects best fit by pure H, pure He, and mixed H/He atmosphere models, respectively. For the eight objects with undetermined compositions, velocities were calculated assuming the pure H solution for simplicity. The choice of the pure H or pure He solution has a negligible effect on the final UVW velocities (see Table 2).

J2137+1050 shows velocities inconsistent with thick disc objects in U, consistent with the analysis in Kilic et al. (2010a), while the results for the J2145+1106 common-proper motion binary are consistent to 2σ, but not 3σ. In addition, three other targets in our sample show velocities inconsistent with thick disc objects: J0822+3903, J1024+4920, and J1513+4743, with cooling ages of 8.5, 6.8, and 2.3 Gyr, respectively. The Toomre diagram for our targets is shown in Fig. 10, with thin disc and thick disc boundaries from Fuhrmann (2004); the differentiation between our halo candidates and the rest of our sample is clearer here than in Fig. 9.

The total main-sequence+white dwarf cooling ages of these objects are relatively young for halo objects, but without parallax measurements, we cannot constrain their masses, velocities, and cooling ages precisely. For example, if these objects have $M \approx 0.53\,M_\odot$ (Bergeron 2001), the progenitor mass would be closer to $1\,M_\odot$ and their main-sequence lifetimes would be on the order of 10 Gyr, making them excellent candidates for membership in the halo. A lower surface gravity would also imply a larger and more distant white dwarf, and UVW velocities that are even more inconsistent with the thick disc population. Conversely, for
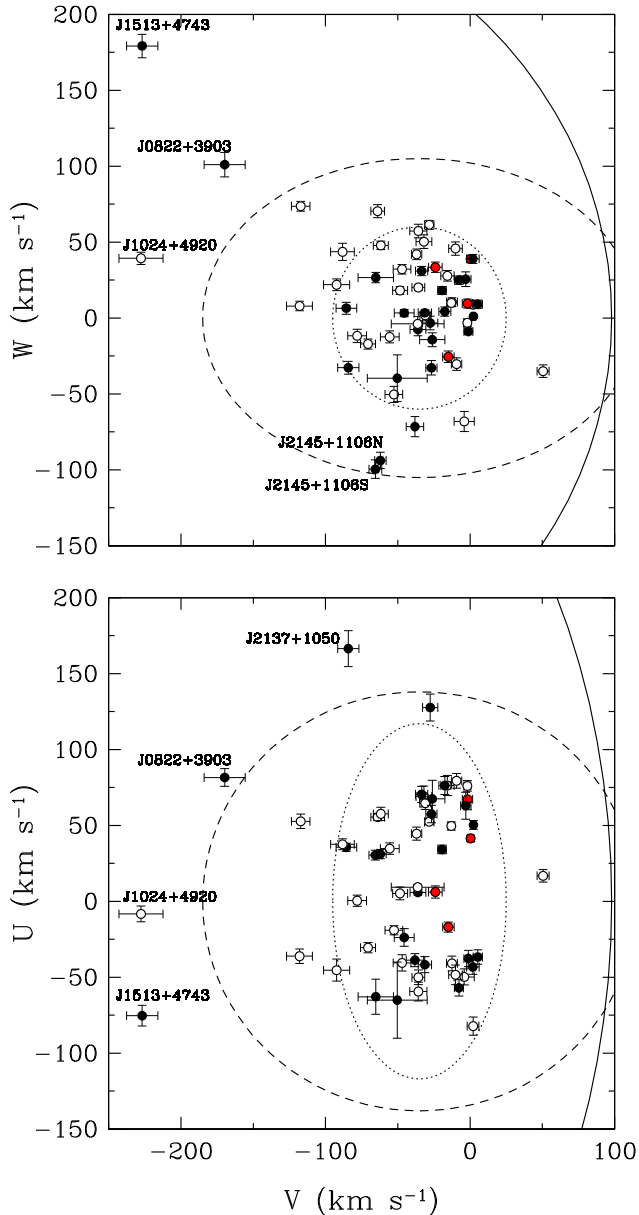
Figure 9. Plots of *W* versus *V* (top) and *U* versus *V* (bottom) velocity distributions for our sample of H-rich (black dots), He-rich (white dots), and mixed (red) white dwarfs. Also plotted are the 3σ ellipsoids for the Galactic thin disc (dotted), thick disc (dashed), and stellar halo populations (solid).

$\log g = 8.5$ white dwarfs, the cooling ages would range from 5 to 11 Gyr, and the *UVW* velocities of our halo white dwarf candidates would remain inconsistent with thick disc objects.

Interestingly, with the exception of the three previously published white dwarfs (J2137+1050 and J2145+1106 binary), none of our objects with cooling ages above 9 Gyr has *UVW* velocities inconsistent with the thick disc, nor do they show the high tangential velocities expected for halo objects. In fact, the highest tangential velocity for these objects is 72 km s^{-1}. Assuming these objects really do belong to the thick disc gives a thick disc age of ≈ 11 Gyr.

Our assumption of zero radial velocity has a negligible effect on our results (see the discussion in Kilic et al. 2010a). The *UVW* velocities of our halo white dwarf candidates remain inconsistent with the 3σ distribution for the thick disc for positive and negative radial velocities up to 100 km s^{-1} (though J0822+3903 only remains inconsistent in both *U* and *W* for radial velocities between -90 and 30 km s^{-1}).

5 CONCLUSIONS

We present follow-up optical spectroscopy and/or near-infrared photometry of 57 cool white dwarf candidates identified from a ≈ 3100 deg^2 proper motion survey described by Munn et al. (2014). 31 of our candidates are spectroscopically confirmed to be white dwarfs, including five DA and 26 DC white dwarfs. The remaining targets have proper motion measurements from both optical and infrared observations that are consistent within the errors. The optical and near-infrared colours for these targets are also consistent with the predictions from the white dwarf model atmospheres. Hence, the contamination from subdwarfs should be negligible for this sample of 57 stars.
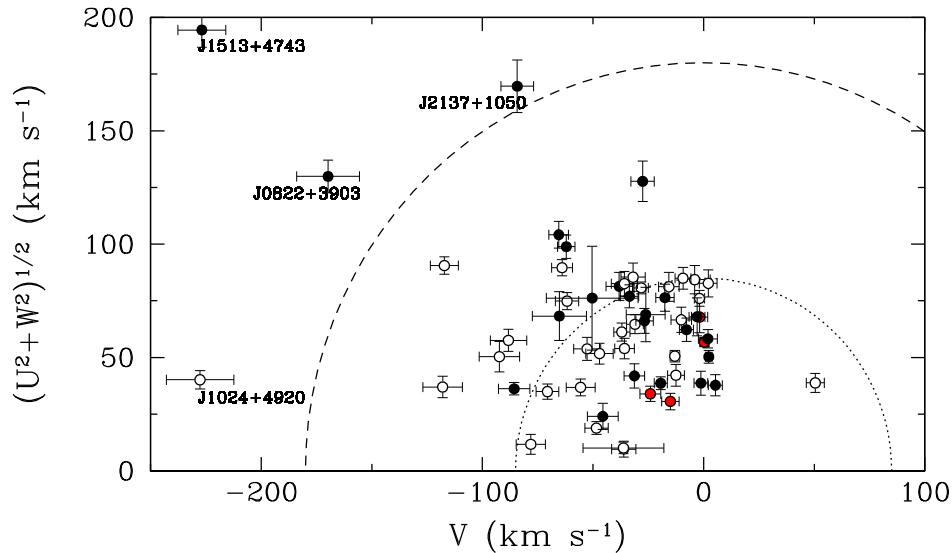
We perform a model atmosphere analysis of these 57 objects using *ugriz* and *JH* photometry. The best-fitting models have 29 pure He atmosphere white dwarfs with $T_{\rm eff} = 4240$–4930 K, 16 pure H atmospheres with $T_{\rm eff} = 3550$–5960 K, and four mixed H/He atmospheres with $T_{\rm eff} = 3210$–3910 K. Eight of our targets lack the near-infrared data necessary to differentiate between the pure H and pure He solutions.

Our sample contains 10 ultracool white dwarf candidates, with another five potential candidates that currently lack near-infrared data. All of the ultracool white dwarfs have hydrogen-rich atmospheres. J1657+2638 is the most interesting with $T_{\rm eff} = 3550 \pm 100$ K and an SED that is reproduced fairly well by a pure H atmosphere. For an average mass of $0.6\,{\rm M_\odot}$, J1657+2638 would be an ≈ 11 Gyr old (main-sequence+cooling age) white dwarf at a distance of 67 pc. The implied tangential velocity of 40 km s^{-1} demonstrates that J1657+2638 belongs to the Galactic thick disc.

Our sample contains three new halo white dwarf candidates. All three have high tangential velocities and *UVW* velocities inconsistent with the Galactic thick disc. The oldest halo white dwarf candidate is J0822+3903 with a cooling age of 8.5 Gyr. However, without trigonometric parallax observations, we cannot accurately constrain the distances, masses, and ages of our white dwarfs.

Our current sample of cool field halo white dwarfs is limited by a lack of deep proper motion surveys. Ongoing and future large-scale surveys such as *Gaia* and LSST will find a significant number of cool white dwarfs, including halo white dwarfs, in the solar neighbourhood. With *g*-band magnitudes of 20–22, we expect parallax errors from *Gaia* to range from about 400–1200 µas,[1] corresponding to uncertainties of ≈ 20 per cent in both mass and cooling age for the majority of our targets. In addition, *Gaia* will reveal the brighter population of halo white dwarfs near the Sun.

---

[1] http://www.cosmos.esa.int/web/gaia/science-performance; GAIA-JBD-022 (for full information, see http://www.cosmos.esa.int/web/gaia/jdb-022)

Figure 10. Toomre diagram for our 57 targets. Symbols have the same meaning as Fig. 9. Thin disc (dotted) and thick disc (dashed) boundaries taken from Fuhrmann (2004).

REFERENCES

Bergeron P., 2001, ApJ, 558, 369
Bergeron P., Leggett S. K., 2002, ApJ, 580, 1070
Bergeron P., Saumon D., Wesemael F., 1995, ApJ, 443, 764
Bergeron P., Leggett S. K., Ruiz M. T., 2001, ApJS, 133, 413
Bergeron P., Ruiz M. T., Hamuy M., Leggett S. K., Currie M. J., Lajoie C.-P., Dufour P., 2005, ApJ, 625, 838
Bergeron P. et al., 2011, ApJ, 737, 28
Brown W. R., McLeod B. A., Geary J. C., Bowsher E. C., 2008, Proc. SPIE, 7014, 70142
Campos F. et al., 2016, MNRAS, 456, 3729
Chiba M., Beers T. C., 2000, AJ, 119, 2843
Fuhrmann K., 2004, Astron. Nachr., 325, 3
Gates E. et al., 2004, ApJ, 612, L129
Gianninas A., Curd B., Thorstensen J. R., Kilic M., Bergeron P., Andrews J. J., Canton P., Agüeros M. A., 2015, MNRAS, 449, 3966
Hansen B. M. S., 1998, Nature, 394, 860
Hansen B. M. S. et al., 2004, ApJS, 155, 551
Hansen B. M. S. et al., 2007, ApJ, 671, 380
Harris H. C. et al., 2006, AJ, 131, 571
Harris H. C. et al., 2008, ApJ, 679, 697
Holberg J. B., Bergeron P., 2006, AJ, 132, 1221
Johnson D. R. H., Soderblom D. R., 1987, AJ, 93, 864
Kalirai J. S., 2012, Nature, 486, 90
Kalirai J. S. et al., 2012, AJ, 143, 11
Kilic M. et al., 2006, AJ, 131, 582
Kilic M. et al., 2010a, ApJ, 715, L21
Kilic M. et al., 2010b, ApJS, 190, 77
Kilic M., Thorstensen J. R., Kowalski P. M., Andrews J., 2012, MNRAS, 423, L132

Kowalski P. M., Saumon D., 2006, ApJ, 651, L137
Lawrence A. et al., 2007, MNRAS, 379, 1599
Leggett S. K., Ruiz M. T., Bergeron P., 1998, ApJ, 497, 294
Liebert J., Dahn C. C., Monet D. G., 1988, ApJ, 332, 891
Liebert J. et al., 2007, in Napiwotzki R., Burleigh M. R., eds, ASP Conf. Ser. Vol. 372, 15th European Workshop on White Dwarfs. Astron. Soc. Pac., San Francisco, p. 129
Munn J. A. et al., 2014, AJ, 148, 132
Oppenheimer B. R. et al., 2001, ApJ, 550, 448
Pauli E.-M., Napiwotzki R., Altmann M., Heber U., Odenkirchen M., Kerber F., 2003, A&A, 400, 877
Pauli E.-M., Napiwotzki R., Heber U., Altmann M., Odenkirchen M., 2006, A&A, 447, 173
Rau A. et al., 2009, PASP, 121, 1334
Richter R., Heber U., Napiwotzki R., 2007, in Napiwotzki R., Burleigh M. R., eds, ASP Conf. Ser. Vol. 372, 15th European Workshop on White Dwarfs. Astron. Soc. Pac., San Francisco, p. 107
Schmidt G. D., Weymann R. J., Foltz C. B., 1989, PASP, 101, 713
Tonry J. L. et al., 2012, ApJ, 745, 42
Tremblay P.-E., Bergeron P., 2009, ApJ, 696, 1755
Tremblay P.-E., Ludwig H.-G., Steffen M., Freytag B., 2013, A&A, 559, A104
Tremblay P.-E., Leggett S. K., Lodieu N., Freytag B., Bergeron P., Kalirai J. S., Ludwig H.-G., 2014, ApJ, 788, 103
Vidrih S. et al., 2007, MNRAS, 382, 515
Winget D. E., Hansen C. J., Liebert J., van Horn H. M., Fontaine G., Nather R. E., Kepler S. O., Lamb D. Q., 1987, ApJ, 315, L77

SUPPORTING INFORMATION

Additional Supporting Information may be found in the online version of this article:

pure_He5.ps
pure_He4.ps
pure_He3.ps
pure_He2.ps
pure_He1.ps
pure_H3.ps
pure_H2.ps

pure_H1.ps
non_IR1.ps
non_IR2.ps
non_IR3.ps

(http://www.mnras.oxfordjournals.org/lookup/suppl/doi:10.1093/mnras/stw2146/-/DC1).

Please note: Oxford University Press is not responsible for the content or functionality of any supporting materials supplied by the authors. Any queries (other than missing material) should be directed to the corresponding author for the article.

This paper has been typeset from a TEX/LATEX file prepared by the author.